Rapidly Solidified Pb-Sn-Ca-Ag Alloy for Electrowinning Anode

M. Kamal[1], R. M. Shalaby[1], T. El Ashram[2], S. M. Abdelaty[2], A. Hany[2],*

[1]Physics Department, Faculty of Science, Mansoura University, Mansoura, Egypt
[2]Physics Department, Faculty of Science, Port-Said University, Port-Said, Egypt
* Corresponding author: amaalamreya@yahoo.com

ABSTRACT

Electrowinning of metals from aqueous solutions has been used for over a century. It is the main recovery method for zinc, gold, silver, copper and cobalt. Lead alloys for anode are widely used because their desirable characteristics like low cost, reducing of power consumption and longer life time. So that the aim of the present work is to study the effect of addition of Ag and rapid solidification using melt spinning technique on the structure, physical and electrochemical properties of Pb-Sn-Ca alloys to be used as anode for electrowinning cell. Six rapidly solidified alloys of Pb-10Sn-2.5Ca-xAg (x = 0, 0.5, 1, 1.5, 2, 2.5 wt.%) were produced by melt-spinning technique. X-ray diffraction analysis and differential scanning calorimetry have been carried out. Also, mechanical, electrical and electrochemical properties were measured. Here we show that adding of Ag to Pb-10Sn-2.5Ca improves its mechanical properties. This is shown in the increase of Young's modulus and micro creep behavior as well as enhancement of corrosion resistance and electrical conductivity. Among the prepared rapidly solidified alloys, the Pb-10Sn-2.5Ca-1.5Ag in wt.% is considered as the one with the best composition to be used as anode for electrowinning cell.

Keywords:

Melt spinning technique, mechanical properties, micro creep, electrical properties, lead alloys, electrowinning.

1. INTRODUCTION

The electrowinning of metals from aqueous solutions has used for over a century. The enhancement of the life time of electrowinning cell depends on the anode material. The important properties of anode alloys for electrowinning cell are good electrical conductivity, high mechanical strength, corrosion resistance and the compatibility with the active materials. Lead based anodes are characterized by good conductivity and high potential, so it is used in the electrowinning of nonferrous metal as copper and zinc [1]. Pb anodes are characterized by

high mechanical strength, so it will not be damaged or deformed during the use [2]. Because of pure lead anode creep, lead must be alloyed with some elements such as Ag, Co, Sb, Ca, Bi and Sr [3].

To minimize cathode contamination, the anode surface must be corrosion resistant before placing of anode in electrowinning process [4]. In cast Pb-Ca-Sn alloys, the calcium content produces large grains with minimal alloy segregation and the calcium content is 0.03-0.08 wt.% to inhibit the formation of Pb_3Ca particles, which cause non uniform corrosion. Also, the addition of calcium enhances the mechanical and electrical properties [5-6]. Tin content in Pb-7Sn anode for chromium plating vary from 6 wt.% to 10 wt.% because the high tin content increase corrosion resistance [7]. Pb-Ca-Sn-Co alloy reduce the use of cobalt in the copper electrolyte to enhance oxygen evolution at the anode [8]. Therefore, the aim of the present work to reveal the effect silver on the structure and properties of Pb-Sn-Ca alloys which are used for anode of electrowinning application.

2. EXPERIMENTAL

Six alloys of compositions Pb-10Sn-2.5Ca-xAg (x= 0, 0.5, 1, 1.5, 2, 2.5 wt.%) were produced by a single copper roller melt-spinning technique (shown in Figure 1). The materials used were from the international company for scientific and medical supplies. The starting purity was better than 99.9%. The quantities of these metals were weighted out (10 g for each composition) and melted in a porcelain crucible and the casting was done in air at 700 °C. The produced ribbons are shown in Figure 2. The speed of the copper wheel was fixed at 2900 rpm, which corresponds to a linear speed of 30.4 ms^{-1}. X-ray diffraction (XRD) analysis was carried out with a Shimadzu X-ray diffractometer (DX-30), using Cu Kα radiation with Ni filter (λ = 0.154056 nm). Differential scanning calorimetry (Shimadzu DSC- 50) was applied with heating rate 10 K/min and the melting temperatures of the produced alloys were calculated. BS407 wide range precision micro- ohmmeter was used to measure the electrical resistivity. A digital Vickers microhardness tester Model-FM-7 was used to measure Vickers microhardness number HV and microcreep as developed and confirmed by T. El Ashram [9-10]. In this method the fractional increase in the area of indentation is considered to be the strain. It was found that this strain increases by increasing the indentation time from which microcreep behavior can be determined. The potentiodynamic current-potential curves were recorded by changing the electrode potential automatically from -500 to 500 mV in case of C-steel with scanning rate 5 mVs^{-1} by using computer controlled potentiostate Gamry PCI4-G750 with DC 105 software for calculations and storted the data.

Figure 1. Melt- spinning technique.

Figure 2. As-quenched melt spun ribbons.

3. RESULTS AND DISCUSSION

3.1. CRYSTAL STRUCTURE

The phases were identified from ICSD using POWD-12++, (1997) [11] and the PDF card number is shown in Table 1. Figure 3. shows the XRD patterns for as-quenched melt-spun ribbons of compositions Pb-10Sn-2.5Ca-xAg (x= 0, 0.5, 1, 1.5, 2, 2.5 wt.%). It shows that the eutectic mixture of Pb and Sn phases up to the composition Pb-10Sn-2.5Ca-1Ag, in which formation of Ag_3Sn intermetallic compound was observed in Pb-10Sn-2.5Ca-1Ag, Pb-10Sn-2.5Ca-1.5Ag and Pb-10Sn-2.5Ca-2Ag alloys. But $CaPb_3$ and Ag_3Sn intermetallic compounds were formed in Pb-10Sn-2.5Ca-1Ag alloy. Ag_3Sn intermetallic compound has orthorhombic crystal system with space group Cmcm but $CaPb_3$ intermetallic compound has cubic crystal system with space group $Pm\bar{3}m$. The Ag_3Sn intermetallic compound is termed Hume-Rothery electron compound because it is formed at certain valence electron concentration ratio (VECR). The VECR for Ag_3Sn formation is 7/4. The $CaPb_3$ is classified as electrochemical compound which is formed due to the difference in electronegativity between Ca and Pb. The variation of lattice parameters and volume of the unit cell of matrix is shown in Table 1. The lattice parameter *a* of Pb matrix was calculated from the peak position of highest intensity which corresponding to the plane (111). The lattice parameter *a* was increased by the addition of Ag from 4.9459 Å for Pb-10Sn-Pb-10Sn-2.5Ca to 4.9489 Å for Pb-10Sn-2.5Ca-0.5Ag alloy and then decreased to 4.9469 Å for Pb-10Sn-2.5Ca-1.5Ag then increased to 4.9489 Å for Pb-10Sn-2.5Ca-2Ag but finally it decreased to the minimum value, 4.9463 Å for Pb-10Sn-2.5Ca-2.5Ag alloy. The decrease in *a* may be due to the dissolving of Ag atom, which has small radius compared to Pb atom. The decrease in *a*, which was observed for Pb-10Sn-2.5Ca-1Ag and Pb-10Sn-2.5Ca-1.5Ag alloys, may be due to the formation of Ag_3Sn intermetallic compound in that alloy. The same behavior was observed for the volume of unit cell *v* of the matrix since $v = a^3$.
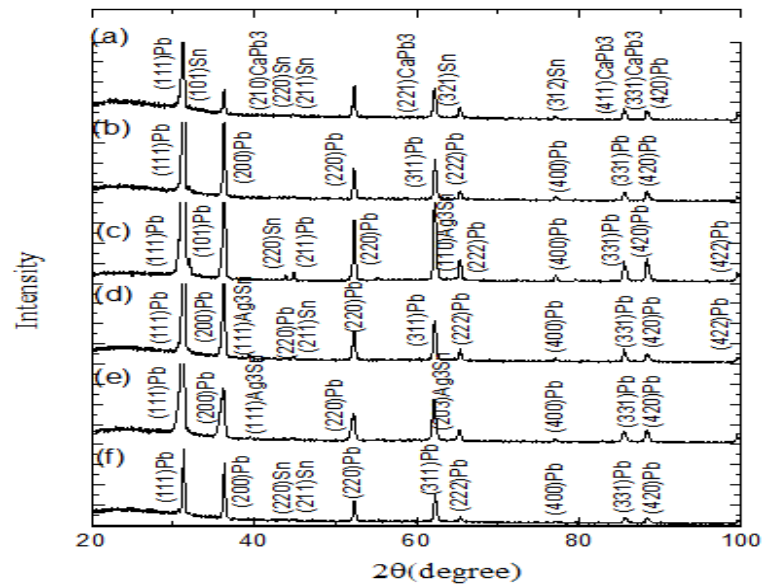
Figure 3. X-ray diffraction pattern of as-quenched melt-spun (a) Pb-10Sn-2.5Ca, (b) Pb-10Sn-2.5Ca-0.5Ag, (c) Pb-10Sn-2.5Ca-1Ag, (d) Pb-10Sn-1.5Ag, (e) Pb-10Sn-2.5Ca-2Ag, (f) Pb-10Sn-2.5Ca-2.5Ag alloys.

Table 1. Details of XRD analysis of Pb-10Sn-2.5Ca-xAg (0, 0.5, 1, 1.5, 2, 2.5 wt. %) alloys.

Alloys	Phases present	Lattice parameter of the matrix Pb a (Å)	Unit cell volume v (Å)3	Cards no.
Pb-10Sn-2.5Ca	Pb Sn CaPb$_3$	4.9459	120.99	01-072-6646 03-065-0296 03-065-8365
Pb-10Sn-2.5Ca-0.5Ag	Pb	4.9489	121.21	01-072-6646
Pb-10Sn-2.5Ca-1Ag	Pb Sn CaPb$_3$ Ag$_3$Sn	4.9476	121.11	01-072-6646 03-065-0296 03-065-8365 00-056-1242
Pb-10Sn-2.5Ca-1.5Ag	Pb Sn Ag$_3$Sn	4.9469	121.06	01-072-6646 03-065-0296 00-056-1242
Pb-10Sn-2.5Ca-2Ag	Pb Ag3Sn	4.9489	121.20	01-072-6646 00-056-1242
Pb-10Sn-2.5Ca-2.5Ag	Pb Sn	4.9463	121.01	01-072-6646 03-065-0296

3.2. THERMAL ANALYSIS

The DSC curves for the three alloys of Pb-10Sn-2.5Ca, Pb-10Sn2.5Ca-1.5Ag and Pb-10Sn-2.5Ca-2.5Ag are shown in Figure 4. In the DSC curves, the melting point is typically calculated by first selecting the most steeping part of the low temperature side of well of the heat absorption, obtaining the slope, then extrapolating the slope line to the temperature at the zero differential heat flow axis. The pasty is defined as the temperature difference between solidus and liquidus temperature. It is found that there is no variation in the decomposition behavior for Pb-10Sn-2.5Ca-1.5Ag and Pb-10Sn-2.5Ca-2.5Ag alloys, as indicated in Figure 4. The addition of Ag decreases the melting temperature (T_m) and slightly increases the enthalpy of fusion (ΔH_f) as shown in Table 2. The melting temperature is the ratio between the enthalpy of fusion and the entropy of fusion. Therefore the decrease in T_m may be due to the increase in entropy which resulted from the large defects and phases introduced in the samples due to the addition of Ag.
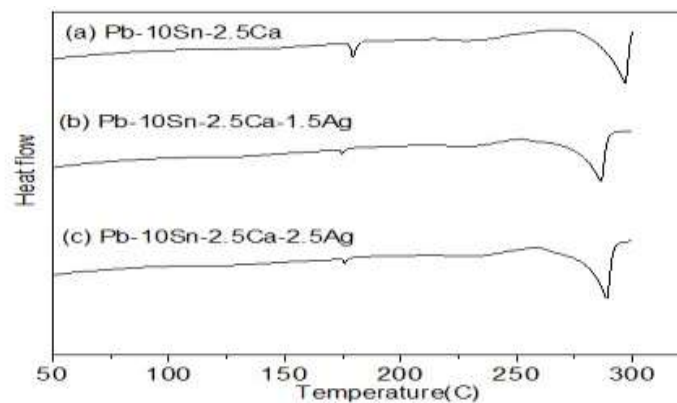

Figure 4. Differential scanning calorimetry (DSC) curves for as-quenched melt- spun Pb-10Sn-2.5Ca-xAg (x= 0, 1.5, 2.5 wt.%) alloys.

Table 2. Details of DSC analysis of as-quenched melt-spun Pb-10Sn-2.5Ca-xAg (x= 0, 1.5, 2.5 wt. %) alloys.

Alloy	T_s (°C)	T_l (°C)	Pasty Range (°C)	T_m (°C)	ΔH (Jg^{-1})
Pb-10Sn-2.5Ca	285.41	305.74	20.33	298.13	29.12
Pb-10Sn-2.5Ca-1.5Ag	274.59	294.19	19.60	287.60	31.73
Pb-10Sn-2.5Ca-2.5Ag	278.48	297.60	19.12	290.26	32.72

3.3. MECHANICAL PROPERTIES

3.3.1. YOUNG'S MODULUS

Figure 5. (a) shows the variation of Young's modulus (E) with the variation of Ag concentration of as-quenched melt-spun Pb-10Sn-2.5Ca-xAg (x=0, 0.5, 1, 1.5, 2, 2.5 wt.%)

alloys. E was decreased by Ag addition from 39.93 GPa for Pb-10Sn-2.5Ca alloy to 20.23 GPa for Pb-10Sn-2.5Ca-0.5Ag then, increased to 40.07 GPa for Pb-10Sn-2.5Ca-1Ag to 50.37 GPa for Pb-10Sn-2.5Ca-1.5Ag alloy and decreased to 25.57 GPa for Pb-10Sn-2.5Ca-2Ag alloy then, it reached to 31.06 GPa for Pb-10Sn-2.5Ca-2.5Ag alloy. The decrease in E may be due to dissolving of Ag atoms in Pb lattice cause attenuation to the bond strength between Pb atoms. The increase in E for 1wt.% and 1.5wt.% Ag can be attributed to formation of $CaPb_3$ and Ag_3Sn intermetallic compounds which are hard phases.

Figure 5. (b) shows the variation of internal friction (Q^{-1}) with the variation of Ag concentration. It shows that the value of Q^{-1} increased with increasing of Ag addition from 0.018 for Pb-10Sn-2.5Ca alloy, reaching the maximum value of 0.189 for Pb-10Sn-2.5Ca-1.5Ag alloy, then decreased to 0.73 for Pb-10Sn-2.5Ca-2Ag then to 0.024 for Pb-10Sn2.5Ca-2.5Ag alloy. The increase in Q^{-1} may be due the motion of substitutional Ag atoms in Pb lattice which have higher mobility due to their smaller size.

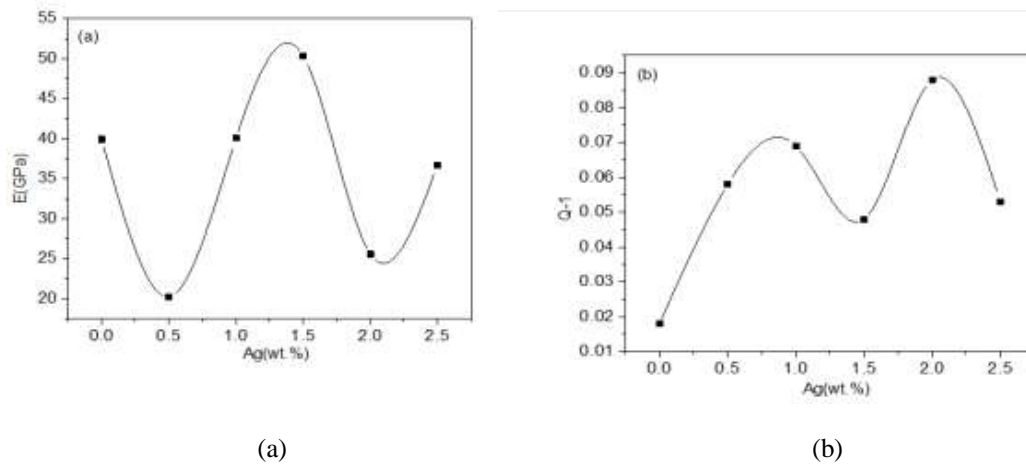(a)   (b)

Figure 5. Variation of (a) Young's Modulus and (b) internal friction with Ca concentration for as-quenched melt-spun Pb-10Sn-2.5Ca-xAg (x= 0, 0.5, 1, 1.5, 2, 2.5 wt.%) alloys.

3.3.2 MICROHARDNESS

Figure 6. shows the variation of HV with Ag concentration of as-quenched melt -spun Pb-10Sn-2.5Ca-xAg (x=0, 0.5, 1, 1.5, 2, 2.5) alloys. HV was found to be 137.69 MPa for Pb-10Sn-2.5Ca alloy. HV decreased by addition of Ag, which was found to be 71.05 MPa for 0.5wt.%Ag. HV was found to be 69.09 MPa for 1wt.% Ag addition and for 1.5wt.% Ag, HV increased to 126.91 MPa. Then HV decreased to 86.73 MPa at 2 wt.% Ag and 74.48 MPa at 2.5wt.%Ag. The decrease of HV may be due to that the solute of Ag atoms in Pb lattice causes local elastic strain which enhance dislocation mobility. The increase of HV may be due to the dispersion of $CaPb_3$ and Ag_3Sn intermetallic compounds, which are hard phases, in the alloy matrix.
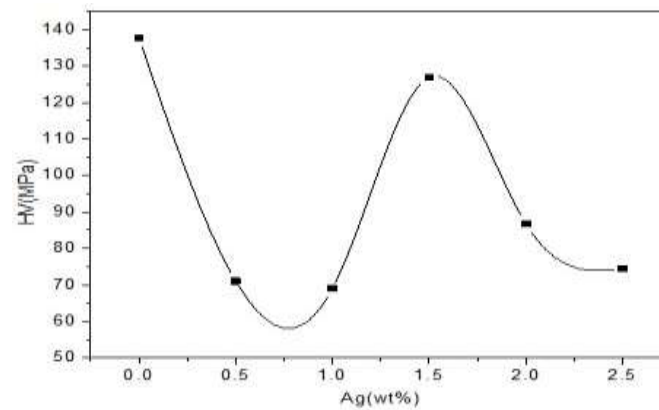
Figure 6. The variation of HV with Ca concentration of as-quenched melt -spun Pb-10Sn-2.5Ca-xAg (x=0, 0.5, 1, 1.5, 2, 2.5 wt.%) alloys.

3.3.3 MICROCREEP

Figure 7. (a) shows the variation of HV with indentation time in time interval from 5 to 99s. It is obvious that HV, for all alloys, decreases by increasing dwell time. Using indentation creep method, we can determine the microcreep behavior. By plotting the strain with indentation time in time interval from 5 to 99 s we obtain Figure 7. (b) which shows the microcreep behavior for as-quenched melt-spun Pb-10Sn-2.5Ca-xAg (x=0, 0.5, 1, 1.5, 2, 2.5 wt.%) alloys. The high creep resistance of these alloys is attributed to the dispersion of $CaPb_3$ and Ag_3Sn intermetallic compounds in the Pb matrix.
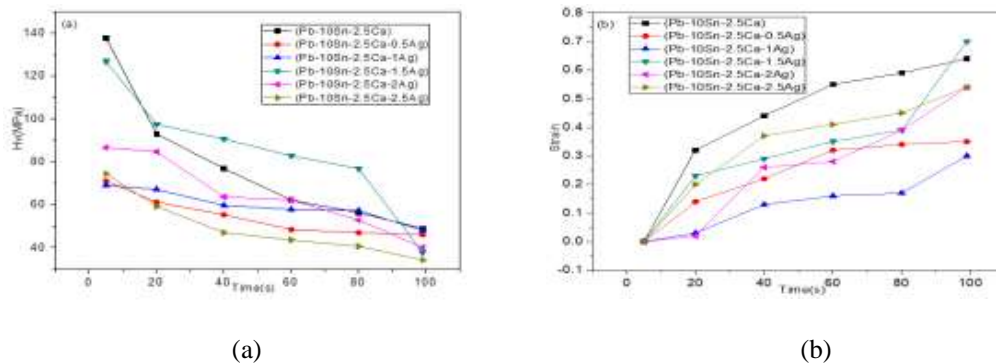

(a)

(b)

Figure 7. The variation of (a)Vickers microhardness number (HV) and (b) strain with dwell time for as-quenched melt-spun Pb-10Sn-2.5Ca-xAg (x=0, 0.5, 1, 1.5, 2, 2.5 wt.%)

3.4 ELECTRICAL RESISTIVITY

The measured electrical resistivity of as-quenched melt -spun Pb-10Sn-2.5Ca-xAg (x=0, 0.5, 1 , 1.5, 2, 2.5 wt. %) alloys, at room temperature, is shown in Table 3. The average dimensions of sample were as the following; length= 4.5 cm, width= 0.3 cm and thickness= 45 μm). The electrical resistivity of Pb-10Sn-2.5Ca alloy was decreased with increasing Ag content this may be attributed to the increase of the number of free electrons due to the addition of Ag.

Table 3. Electrical resistivity variation with Ca concentration of as-quenched melt -spun
Pb-10Sn-2.5Ca-xAg (x=0, 0.5, 1, 1.5, 2, 2.5 wt.%) alloys

Alloy	Electrical Resistivity at RT, $\rho x 10^{-8}$ Ω.m
Pb-10Sn-2.5Ca	29.25
Pb-10Sn-2.5Ca-0.5Ag	30
Pb-10Sn-2.5Ca-1Ag	24.9
Pb-10Sn-2.5Ca-1.5Ag	16.8
Pb-10Sn-2.5Ca-2Ag	21.4
Pb-10Sn-2.5Ca-2.5Ag	28.9

3.5 ELECTROCHEMICAL BEHAVIOR

Potentiodynamic polarization curves for Pb-10Sn-2.5Ca-xAg (x=0, 0.5, 1, 1.5, 2, 2.5 wt.%) alloys in 0.1 N H_2SO_4 are shown in Figure 8. From these curves the corrosion potential E_{Corr} and corrosion current I_{Corr} were determined. Then the corrosion rate was calculated for all alloys as shown in Table 4. It is evident that the corrosion rate decreases by increasing Ag concentration to minimum value about 44.2 mpy for 2.5 Ag alloy. There are many factors affect corrosion such as the chemical composition and concentrations of the material under investigation and its environment, temperature, the crystal structure and microstructure of the material. All these factors were kept constant except the variation of Ag concentration. Therefore, Ag atoms may act as corrosion inhibitors in Pb-Sn-2.5Ca alloy. This means that the addition of Ag atoms to enhances the corrosion resistance of Pb-10Sn-2.5Ca alloys.
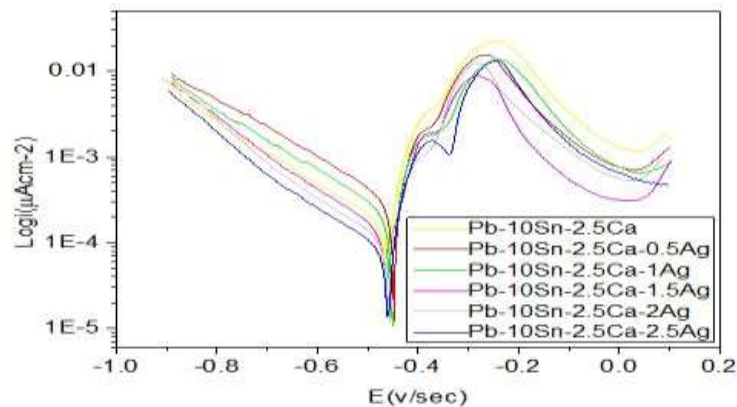

Figure 8. Potentiodynamic polarization curves for Pb-10Sn-2.5Ca-xAg (x=0, 0.5, 1, 1.5, 2, 2.5 wt.%) alloys in 0.1 N H_2SO_4

Table 4. corrosion potential E_{Corr} , corrosion current I_{Corr} and corrosion rate of Pb-10Sn-

Alloy	I_{Corr} ($\mu A\ cm^{-2}$)	$-E_{Corr}$ (mV)	C. R (mpy)
Pb-10Sn-2.5Ca	224	462	95.98
Pb-10Sn-2.5Ca-0.5Ag	369	448	158.4
Pb-10Sn-2.5Ca-1Ag	256	454	110.68
Pb-10Sn-2.5Ca-1.5Ag	142	458	60.97
Pb-10Sn-2.5Ca-2Ag	131	458	56.31
Pb-10Sn-2.5Ca-2.5Ag	103	459	44.20

2.5Ca-xAg (x=0, 0.5, 1, 1.5, 2, 2.5 wt.%) alloys in 0.1N H_2SO_4

4. CONCLUSION

The obtained results show that the addition of Ag to Pb-10Sn 2.5Ca alloy improves the electrical properties as well as the associated mechanical properties. This is evident in the increase of Young's modulus, microcreep behavior and the enhancement of corrosion resistance. Therefore, the rapidly solidified melt-spun Pb-10Sn-2.5Ca-1.5Ag in wt.% can be promising alloy as anode in electrowinning cell.

REFERENCES

[1] Tunnicliffe M, Mohammadi F, Alfantazi A. Polarization behavior of lead-silver anodes in zinc electrowinning. Journal of Electrochemical Society. 4 (2012) 159.

[2] Schlesingeer M E, King M J, Sole K C, et al. Extractive Metallurgy of Copper [M]. 5th E. The Netherlands, (2011) 360-369.

[3] J.A. Gonzalez, J. Rodrigues, and A. Siegmund, "Advances and Application of Lead Alloy Anodes for Zinc Electrowinning," (Tokyo: Mining and Materials Processing Institute of Japan 2 (2005) 1046.

[4] Jose Alberto Gonzalez, Jo Rodrigues, Andreas Siegmund , Anode paper ,2005.

[5] . R.D. Prengaman, "The Metallurgy and Performance of Cast and Rolled Lead Alloys for Battery Grids," Journal of Power Sources, 67 (1997) 267.

[6] A. Siegmund and R.D. Prengaman, "New Wrought Pb-Ag-Ca Anodes for Zinc Electrowinning to Produce a Protective Oxide Coating Rapidly," Lead-Zinc 2000, ed. J.E. Dutrizac et al. (2000) 589–597.

[7] W. Blum and G. Hogaboom, Principles of Electroplating and Electroforming (New York: McGrawHill Book Company, (1958) 343-344.

[8] Aaron Felder and R. David Prengaman, Lead Alloys for Permanent Anodes in the Nonferrous Metals Industry, (2006) 28-31.

[9] T. El-Ashram, R.M. Shalaby, J. Electron. Mater. 34 (2005) 212–215.

[10] Mustafa Kamal, Tarek El Ashram, Materials Science and Engineering A 456 (2007) 1–4.

[11] Calculated from ICSD using POWD-12++, 1997.